Ocean Engineering 121 (2016) 37–46

Contents lists available at ScienceDirect

Ocean Engineering

journal homepage: www.elsevier.com/locate/oceaneng

Decomposition model for naval hydrodynamic applications, Part I: Computational method

Vuko Vukčević [a,*], Hrvoje Jasak [a,b], Šime Malenica [c]

[a] University of Zagreb, Faculty of Mechanical Engineering and Naval Architecture, Ivana Lučića 5, Zagreb, Croatia
[b] Wikki Ltd, 459 Southbank House, SE1 7SJ, London, United Kingdom
[c] Bureau Veritas, 67/71, 92200 boulevard du Château, Neuilly-sur-Seine, France

ARTICLE INFO

Article history:
Received 21 April 2015
Received in revised form
22 March 2016
Accepted 10 May 2016

Keywords:
Solution and domain decomposition
SWENSE
Wave modelling
Implicitly redistanced Level Set
Collocated finite volume method
OpenFOAM

ABSTRACT

The present paper and its companion present a solution and domain decomposition model for general two-phase, incompressible and turbulent flows encountered in naval hydrodynamics. The mathematical and numerical model are derived within the framework of polyhedral finite volume method. Interface capturing is obtained with implicitly redistanced level set method derived from the phase field equation. This approach removes the need to redistance the level set field, thus saving CPU time and increasing numerical stability. A modified, Spectral Wave Explicit Navier–Stokes Equations method is introduced and used for wave modelling, where the solution is decomposed into incident and perturbation fields. The incident field is readily available from potential flow theories, and only the perturbation component is solved within the non-linear equation set of the free surface flow model. The domain is decomposed with implicit relaxation zones used to prevent wave reflection by forcing the perturbation fields to vanish in the far-field. A second-order, collocated finite volume method is used to discretise the equations. All equations are solved implicitly, which enables the use of higher Courant–Friedrichs–Lewy numbers compared to explicit scheme. The algorithm is implemented in foam-extend-3.1, a community driven fork of the OpenFOAM CFD software. Verification and validation of the model is presented in the accompanying paper.

1. Introduction

Over the past decades, Computational Fluid Dynamics (CFD) is progressively gaining attention in the naval hydrodynamics community due to increased computer resources and ability to handle non-linear model equation sets. Recently, Stern et al. (2012) presented an overview of the capabilities of CFD for a wide range of phenomena related to naval hydrodynamics. Nevertheless, there is an ongoing effort to validate CFD codes (Larsson et al., 2013), for both steady and transient simulations. A large portion of transient naval hydrodynamic flows is concerned with ocean waves and their interaction with ships and offshore structures. For this reason, we present a general decomposition method for the incompressible, two-phase and turbulent flow model in the vicinity of the object of interest.

Free-surface flows are often modelled by Navier–Stokes equations. A number of approaches for free-surface flow modelling exist (Tryggvason et al., 2011): Volume of Fluid (VOF) (Ubbink and Issa, 1999), Lagrangian tracking and Level Set (LS) methods (Sethian, 1996). Although VOF is conservative and well established, special care has to be taken to ensure boundedness and capturing of a sharp interface. Smearing of the interface in the VOF method is often remedied with special compressive schemes (Ubbink, 1997; Ubbink and Issa, 1999) or additional compressive terms (Rusche, 2002). In the LS method, smearing of the interface is a user-controlled parameter. The LS method is often based on the signed distance function (Osher and Fedkiw, 2003) which does not represent a conserved physical quantity. Moreover, the LS field may not preserve its signed distance property due to discretisation errors when it is advected by a velocity field obtained from the pressure–velocity system. This is often remedied by introducing an additional redistancing equation (Sussman and Fatemi, 1999) or directly recalculating the distance to the interface after the advection step. Both methods usually redistance the LS field only in a narrow band of interest near the interface.

In this paper, we take a different approach: using the LS equation derived from the phase field (PF) equation (Sun and Beckermann, 2007, 2008). The PF equation contains additional

* Corresponding author.
E-mail addresses: vuko.vukcevic@fsb.hr (V. Vukčević), hrvoje.jasak@fsb.hr, h.jasak@wikki.co.uk (H. Jasak), sime.malenica@bureauveritas.com (Š. Malenica).

http://dx.doi.org/10.1016/j.oceaneng.2016.05.022
0029-8018/

terms along with the usual advection which serve to maintain the signed distance property implicitly during the solution (Sun and Beckermann, 2007). Hence, no additional redistancing is needed.

The LS method is very suitable for a solution decomposition as used in this work. This decomposition is achieved using the Spectral Wave Explicit Navier–Stokes Equations (SWENSE) method (Ferrant et al., 2002; Ducrozet et al., 2014), where the unknown fields representing the free surface and velocity are decomposed into incident and perturbation components. A similar methodology has been recently used to investigate wave resonance in a narrow gap between two barges in fully non-linear potential flow framework (Feng and Bai, 2015). The incident component of a given field is obtained from potential flow models, while the perturbation component is solved for. This method was successfully applied to both calm water, regular and irregular waves (Monroy et al., 2010; Marcer et al., 2007). In their work, Monroy et al. (2010) used fully non-linear potential flow theories, such as stream function solution for regular waves (Rienecker and Fenton, 1981) and higher order spectrum (HOS) (West et al., 1987; Dommermuth and Yue, 1987) for irregular seas. Here, we present a modification of the original SWENSE approach (Ferrant et al., 2002), consistent with properties of the second-order Finite Volume (FV) method. This enables the use of linear potential flow theories, which makes the simulations of irregular sea states possible without advanced models such as HOS.

Wave modelling in CFD requires special treatment in order to prevent wave reflection and pollution of the results. Higuera et al. (2013a,b) used active wave absorption by dynamically prescribing the velocity field on the outlet boundaries. This approach may be favourable for simulations in closed domains (i.e. experimental set-up). In naval and offshore applications, the area of interest often lies within a narrow region near an object. For this reason, we turn our focus to damping regions.

Huang et al. (2007) used a damping source term in the LS interface capturing equation to prevent wave reflection. Jacobsen et al. (2012) applied explicit relaxation zones to achieve the same effect. Here, we use relaxation zones with implicit matrix blending as described by Jasak et al. (2015). Inside relaxation zones, we gradually force the perturbation fields to zero, leaving only potential flow solution in the far field, thus preventing wave reflection. Higuera et al. (2013a) consider this approach inferior due to a larger domain needed to accommodate for relaxation zones. The cells in the relaxation zones are usually very large, which is favourable as this increases numerical dissipation. In addition, possible use of advanced potential flow theories allows us to model only small area near the object of interest without a detrimental effect on the solution.

Numerical discretisation is achieved with a second-order accurate, collocated, polyhedral FV method implemented in foam-extend, a community driven fork of the OpenFOAM CFD software. OpenFOAM (Weller et al., 1998) is an open source object-oriented C++ library for general numerical computational continuum mechanics, that provides efficient linear system solvers and support for massively parallel computations by domain decomposition. All governing equations are discretised implicitly, leading to stable simulations even at high Courant–Friedrichs–Lewy (CFL) numbers. Special care is given to the consistency and implicitness of the FV discretisation of the LS equation. Coupling of pressure, momentum and Level Set equations is resolved in a segregated way using an algorithm similar to a combination of SIMPLE (Patankar and Spalding, 1972) and PISO (Issa, 1986).

The paper is organised as follows. Mathematical model of incompressible, turbulent flow is presented in Section 2. Free surface flow modelling is described in Section 3, with emphasis on the LS method derived from PF equation. SWENSE decomposition and implicit blending technique for wave generation and absorption are discussed in detail in Section 4. The description of FV discretisation is followed by the analysis of the solution algorithm in Section 5. Verification, validation and the performance of the method are reported in the accompanying paper.

2. Mathematical model

This section presents the mathematical model of free surface, incompressible flow used in this work. The model is based on the equations for continuity and momentum (Navier–Stokes equations). The incompressible, Newtonian fluid model is used, which is a justified assumption for low speed, wave-like phenomena of interest in this work. Considerations presented here allow the use of general turbulence models (Wilcox, 1993). However, turbulence can often be neglected in case of mild, non-breaking waves. The following governing equations are of mixture type, which means that all fields are defined in both phases (water and air) and are assumed continuous across the interface.

2.1. Mixture equations

Density ρ, dynamic viscosity μ, and velocity $\mathbf{u}$ of the mixture are defined with the assumption of linear variation with respect to volume fraction, α:

$$\rho = \alpha\rho_1 + (1-\alpha)\rho_2, \tag{1}$$

$$\mu = \alpha\mu_1 + (1-\alpha)\mu_2, \tag{2}$$

$$\mathbf{u} = \alpha\mathbf{u}_1 + (1-\alpha)\mathbf{u}_2, \tag{3}$$

where index 1 indicates the properties in the first phase (e.g. water) and index 2 the properties in the second phase (e.g. air). The relation between the LS signed distance field ψ and volume fraction α will be given in Section 3.

2.2. Continuity and momentum equations

The continuity equation in continuum mechanics reads:

$$\frac{\partial\rho}{\partial t} + \nabla\cdot(\rho\mathbf{u}) = 0. \tag{4}$$

Assuming a linear variation of ρ with α, Eq. (1), Ubbink (1997) shows that Eq. (4) reduces to the volumetric continuity equation for mixture velocity:

$$\nabla\cdot\mathbf{u} = 0. \tag{5}$$

Consider the mixture momentum equation at rest (Vukčević et al., 2014). Giving a balance of static pressure and volumetric body force:

$$p = \rho\mathbf{g}\cdot\mathbf{x}, \tag{6}$$

since

$$\nabla p = \rho\mathbf{g}. \tag{7}$$

The volumetric body force represented by the $\rho\mathbf{g}$ source term is problematic for numerical reasons: we shall proceed by reformulating it as a gradient term. In Section 5, it will be shown that the gradient form allows us to control the computational stencil; this will give identical support stencil for the source term due to gravity as for the pressure gradient. This is achieved by the decomposition of the pressure into a hydrostatic $\rho\mathbf{g}\cdot\mathbf{x}$ and a dynamic p_d part:

$$p = p_d + \rho \mathbf{g} \cdot \mathbf{x}, \tag{8}$$

where $\mathbf{g}$ is the gravitational acceleration and $\mathbf{x}$ is the position vector. Note that ρ is the current density field, meaning that the decomposition of p changes with motion of the free surface. Inserting Eq. (8) into term pairing given by Eq. (7) results in:

$$-\nabla p + \rho \mathbf{g} = -\nabla p_d - (\mathbf{g} \cdot \mathbf{x} \nabla \rho), \tag{9}$$

In Section 5, the pressure equation will be formulated from Eq. (5) in terms of p_d, while p can be reconstructed using Eq. (8). With this decomposition, the mixture momentum equation for the two-phase flow becomes:

$$\frac{\partial(\rho \mathbf{u})}{\partial t} + \nabla \cdot (\rho \mathbf{u}\mathbf{u}) - \nabla \cdot (\mu_{eff} \nabla \mathbf{u}) = -\nabla p_d - \mathbf{g} \cdot \mathbf{x} \nabla \rho + \nabla \mathbf{u} \cdot \nabla \mu_{eff} + \sigma \kappa \nabla \alpha, \tag{10}$$

where μ_{eff} denotes the effective dynamic viscosity from turbulence modelling. Additional terms on the right-hand side of the equation come from the variation of dynamic viscosity across the interface and the Continuum Surface tension Force (CSF) model by Brackbill et al. (1992). A detailed derivation of Eq. (10) is given by Ubbink (1997).

3. Interface capturing

Free surface flow modelling in CFD is most often achieved with interface capturing or Lagrangian interface tracking methods (Tryggvason et al., 2011). Most of the latter methods use Lagrangian points to advect the interface without loss of sharpness, while the former often use a form of colour function to denote the location of the interface. The colour function is then advected to follow the motion of the interface. Interface capturing methods often diffuse (smear) the interface over a few computational points to ensure numerical stability. Although it is possible to reconstruct the sharp interface from the colour function, there is no need for this if smearing of the interface is confined to a small region. Interface capturing methods can be divided into three major groups:

1. Level Set (LS) methods (Osher and Fedkiw, 2003; Sethian, 1996);
2. Phase Field (PF) methods (Sun and Beckermann, 2007, 2008);
3. Volume of Fluid (VOF) methods (Ubbink and Issa, 1999; Ubbink, 1997; Rusche, 2002),

as presented in Fig. 1. Two phases, Ω_1 and Ω_2, are separated by a free surface (Γ).

3.1. Level Set method

The LS method uses the signed distance function to capture the interface:

$$\psi(\mathbf{x}) = \begin{cases} d, & \text{if } \mathbf{x} \in \Omega_1, \\ 0, & \text{if } \mathbf{x} \in \Gamma, \\ -d, & \text{if } \mathbf{x} \in \Omega_2, \end{cases} \tag{11}$$

where d is the shortest Euclidean distance to the interface and $\mathbf{x}$ is the position vector. The interface is reconstructed with zero level set $\psi(\mathbf{x}) = 0$. The signed distance function is not bounded, as opposed to VOF and PF, making it more convenient to advect using second order FV method. However, the signed distance function has a linear profile in hydrostatic case, which is unfavourable from numerical perspective.

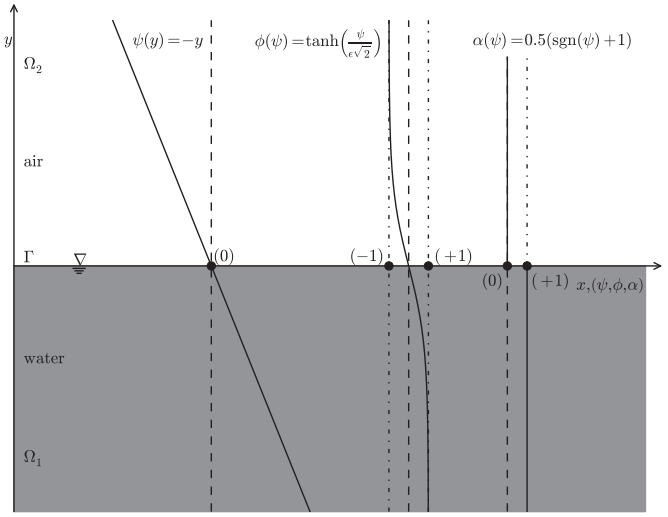

Fig. 1. Comparison of interface capturing schemes. ψ is the signed distance function for the Level Set field, ϕ is the Phase Field and α is the volume fraction in the Volume of Fluid approach.

3.2. Phase Field method

The PF is bounded between −1 and 1 with a prescribed hyperbolic tangent profile across the interface, which in turn depends on the signed distance function:

$$\phi(\psi) = \tanh\left(\frac{\psi}{\epsilon\sqrt{2}}\right), \tag{12}$$

where the width parameter ϵ controls the smearing of the interface. It is important to note that the smearing of the interface in Eq. (12) is a user controlled parameter. For example, Sun and Beckermann (2007) show that ϕ varies from −0.9 to 0.9 over $3\sqrt{2}\epsilon$. The interface is reconstructed in the same way as in the LS method, $\phi(\mathbf{x}) = 0$.

3.3. Volume of Fluid method

The VOF method represents a fraction of the volume occupied by water inside an arbitrary control volume. It defines a sharp interface according to LS field:

$$\alpha(\psi) = 0.5(\mathrm{sgn}(\psi) + 1), \tag{13}$$

where $\mathrm{sgn}(\psi)$ denotes the signum function. However, the initially sharp interface often gets smeared due to numerical discretisation of bounded convection terms. Reconstruction of the interface in the VOF method is a computationally challenging task, especially for unstructured polyhedral grids. Nevertheless, Luppes et al. (2012) and Kleefsman (2005) apply it successfully on Cartesian grids. Using Eq. (13) to calculate fluid properties from Eqs. (1) and (2) causes numerical instabilities. Hence, we use a combination of Eqs. (12) and (13) to artificially smear the interface in a prescribed way:

$$\alpha(\psi) = 0.5\left(\tanh\left(\frac{\psi}{\epsilon\sqrt{2}}\right) + 1\right). \tag{14}$$

The width parameter ϵ is chosen to smear the interface across two or three cells. This gives sufficient accuracy and numerical stability.

3.4. Level set transport equation

The solution of the usual advection equation for the LS field

does not guarantee the preservation of the signed distance function. Moreover, the field may get so distorted that a redistancing algorithm is needed. Redistancing algorithms (Gómez et al., 2005; Hartmann et al., 2008; Sussman and Fatemi, 1999) often redistance the LS field after solving the transport equation, increasing the computational cost and causing potential phase conservation issues. Recently, Sun and Beckermann (2007) have derived a transport equation for PF that preserves the hyperbolic tangent character given by Eq. (12). Eq. (12) also presents a mapping between the PF ϕ and the LS ψ. This identity is used to derive a transport equation for the LS field from the PF equation presented by Sun and Beckermann (2007). The resulting equation has the following form:

$$\frac{\partial \psi}{\partial t} + \mathbf{u} \cdot \nabla \psi = b\left(\nabla \cdot (\nabla \psi) + \frac{\sqrt{2}}{\epsilon}(1 - |\nabla \psi|^2) \tanh\left(\frac{\psi}{\epsilon \sqrt{2}} \right) - |\nabla \psi| \nabla \cdot \left(\frac{\nabla \psi}{|\nabla \psi|} \right) \right). \quad (15)$$

We will briefly discuss the terms in Eq. (15); the reader is referred to Sun and Beckermann (2007) for a detailed derivation and analysis. The terms on the left-hand side (LHS) represent advection. The first term on the right-hand side (RHS) is a diffusion term that serves to smooth out possible singularities. The second term on the RHS is the curvature-driven motion of the interface. In the air–water two-phase system at naval hydrodynamics length-scale, this term could be neglected because of the fluid properties. The third term counteracts the second term. Folch et al. (1999) show that the inclusion of second and third terms is numerically beneficial, even though they represent the same physical phenomena. In the absence of curvature-driven motion, b is no more than a numerical parameter: it will be defined in Section 5.

4. SWENSE decomposition

The original SWENSE method (Ferrant et al., 2002) decomposes the fields into incident and diffracted (perturbation) components. An arbitrary field of interest (ξ) can be decomposed as:

$$\xi = \xi_I + \xi_P, \quad (16)$$

where index I denotes incident field and P denotes perturbation field. ξ_I may in theory be an arbitrary field, and ξ_P should adjust accordingly to satisfy the governing equation. Note that in the present model, ξ_P does not only account for wave diffraction, it also accounts for non-linear, two-phase, viscous effects. To be precise, ξ_P models all the effects not present in the incident flow model.

The idea of SWENSE decomposition is to capture main features of free surface waves with a potential flow model, providing ξ_I, and superimpose non-linear, viscous and turbulent effects by extending ξ_I to a full Navier–Stokes model via ξ_P. We shall proceed by deriving the mathematical model for ξ_P under an arbitrary choice of ξ_I. However, from the computational perspective, it is desirable to have ξ_I to be as close to ξ as possible. Such decomposition is desirable since the incident wave field can often be very close to the desired solution. Moreover, neglecting rotational motion and viscosity provides potential flow theories significant speed up compared to CFD simulations.

4.1. Continuity and momentum equations

The decomposed volumetric continuity equation, Eq. (4), is:

$$\nabla \cdot \mathbf{u}_P = -\nabla \cdot \mathbf{u}_I. \quad (17)$$

It should be noted that $\nabla \cdot \mathbf{u}_I$ is zero in potential flow. Nevertheless, this identity is valid at differential level (for Stokes' wave theories) and arbitrary numerical level (stream function or higher order spectrum) in discrete form. On an arbitrary CFD mesh, there is no guarantee that $\nabla \cdot \mathbf{u}_I$ will be zero (see Fig. 4 in Section 5), and the term on the RHS of Eq. (17) is kept.

The decomposition of the momentum equation, Eq. (10), reads:

$$\begin{aligned} &\frac{\partial(\rho \mathbf{u}_P)}{\partial t} + \nabla \cdot (\rho \mathbf{u}\mathbf{u}_P) - \nabla \cdot (\mu_{eff} \nabla \mathbf{u}_P) \\ &= -\frac{\partial(\rho \mathbf{u}_I)}{\partial t} - \nabla \cdot (\rho \mathbf{u}\mathbf{u}_I) + \nabla \cdot (\mu_{eff} \nabla \mathbf{u}_I) - \nabla p_d - \mathbf{g} \cdot \mathbf{x} \nabla \rho \\ &\quad + \nabla \mathbf{u} \cdot \nabla \mu_{eff} + \sigma \kappa \nabla \alpha. \end{aligned} \quad (18)$$

This decomposition is different from one presented by Ferrant et al. (2002) for several reasons. The velocity field is only decomposed in time derivative, convection and diffusion terms. Other terms are treated explicitly in the numerical algorithm (see Section 5) and no decomposition is necessary. This is valid because the entire velocity field $\mathbf{u}$ is reconstructed at the end of each time-step. The convecting velocity field in the convection term is not decomposed because the convection term is linearised using the explicit mass flux $\rho \mathbf{u}$, from the previous time-step. Decomposing all terms would result in the Euler equation (Ferrant et al., 2002) for incident field. The Euler equation is satisfied in the potential flow models: incident field terms could be neglected. However, for the same reason as for the continuity equation, Eq. (17), the terms are included in the system.

Decomposition of p_d would yield two pressure equations (one for incident and one for perturbation field) by separately forcing $\nabla \cdot \mathbf{u}_P$ and $\nabla \cdot \mathbf{u}_I$ to vanish. Due to its elliptic nature in incompressible flows, the pressure equation is often the most time-consuming part of a CFD algorithm. Hence, the dynamic pressure is not decomposed for efficiency reasons. Eq. (17) will be used to formulate the dynamic pressure equation as described in Section 5.

4.2. Level set equation

Free surface description via VOF and PF is unsuitable for SWENSE decomposition due to their boundedness, and, in case of VOF, sharp jump of α at the interface. For this reason, we shall decompose LS transport equation, Eq. (15).

Prior to decomposition, Eq. (15) is written in a form more suitable for strongly conservative FV discretisation. The last two terms on the RHS of Eq. (15) can be expanded as:

$$\begin{aligned} -b\frac{\sqrt{2}}{\epsilon} \tanh\left(\frac{\psi}{\epsilon \sqrt{2}} \right) |\nabla \psi|^2 &= -b\frac{\sqrt{2}}{\epsilon} \tanh\left(\frac{\psi}{\epsilon \sqrt{2}} \right) \nabla \psi \cdot \nabla \psi \\ &= -\mathbf{w}_1 \cdot \nabla \psi = -\nabla \cdot (\mathbf{w}_1 \psi) + \psi \nabla \cdot \mathbf{w}_1, \end{aligned} \quad (19)$$

where the second identity introduces $\mathbf{w}_1$ as:

$$\mathbf{w}_1 = b\frac{\sqrt{2}}{\epsilon} \tanh\left(\frac{\psi}{\epsilon \sqrt{2}} \right) \nabla \psi, \quad (20)$$

which is an additional term that transports the LS field. The procedure for the last term in Eq. (15) is similar and yields:

$$\begin{aligned} -b\nabla \cdot \left(\frac{\nabla \psi}{|\nabla \psi|} \right) |\nabla \psi| &= -b\kappa |\nabla \psi| = -b\kappa \frac{\nabla \psi}{|\nabla \psi|} \cdot \nabla \psi = -\mathbf{w}_2 \cdot \nabla \psi \\ &= -\nabla \cdot (\mathbf{w}_2 \psi) + \psi \nabla \cdot \mathbf{w}_2, \end{aligned} \quad (21)$$

where κ is the mean interface curvature and $\mathbf{w}_2$ is an additional term that transports the LS field:

$$\mathbf{w}_2 = b\kappa \frac{\nabla \psi}{|\nabla \psi|}. \quad (22)$$

Inserting Eqs. (19) and (21) into Eq. (15) gives:

$$\frac{\partial \psi}{\partial t} + \mathbf{u} \bullet \nabla \psi + \nabla \bullet (\mathbf{w}_1 \psi) - \psi \nabla \bullet \mathbf{w}_1 + \nabla \bullet (\mathbf{w}_2 \psi) - \psi \nabla \bullet \mathbf{w}_2 - b \nabla \bullet (\nabla \psi) = b \frac{\sqrt{2}}{\epsilon} \tanh\left(\frac{\psi}{\epsilon \sqrt{2}} \right). \tag{23}$$

Using the volumetric continuity equation, Eq. (5), convective terms can be grouped together:

$$\frac{\partial \psi}{\partial t} + \nabla \bullet (\mathbf{c} \psi) - \psi \nabla \bullet \mathbf{c} - b \nabla \bullet (\nabla \psi) = b \frac{\sqrt{2}}{\epsilon} \tanh\left(\frac{\psi}{\epsilon \sqrt{2}} \right), \tag{24}$$

where $\mathbf{c} = \mathbf{u} + \mathbf{w}_1 + \mathbf{w}_2$ is the modified convective velocity field that transports and maintains the signed distance function with the help of diffusion and source terms. This form of the LS transport equation is favourable from a numerical perspective because source terms are reformulated to divergence terms.

SWENSE decomposition of Eq. (24) gives:

$$\frac{\partial \psi_P}{\partial t} + \nabla \bullet (\mathbf{c} \psi_P) - \psi_P \nabla \bullet \mathbf{c} - b \nabla \bullet (\nabla \psi_P) = -\frac{\partial \psi_I}{\partial t} - \nabla \bullet (\mathbf{c} \psi_I) + \psi_I \nabla \bullet \mathbf{c} + b \nabla \bullet (\nabla \psi_I) + b \frac{\sqrt{2}}{\epsilon} \tanh\left(\frac{\psi}{\epsilon \sqrt{2}} \right), \tag{25}$$

where the last source term is not decomposed since it will not be treated implicitly. Although Picard linearisation is possible (Patankar, 1980), it can be shown that the linearisation of hyperbolic tangent would create a source term. Since the source term is positive on the RHS of the equation, its implicit treatment would decrease the diagonal dominance of the resulting matrix (see Appendix A). This is avoided by treating the term explicitly. Similar to the convective term in the momentum equation, Eq. (18), the convecting field $\mathbf{c}$ is not decomposed.

In the SWENSE decomposition, only the perturbation in ψ around ψ_I is calculated, rather than complete signed distance profile. Thus, linear profile in hydrostatic case does not have to be calculated. This decomposition allows us to efficiently introduce incoming waves in the CFD simulation, by prescribing $\mathbf{u}_I$ and ψ_I at each time step, and solving only for the perturbation component.

4.3. Prevention of the wave reflection: relaxation zones

If perturbation components do not vanish near the boundaries, wave reflection will occur, which will in turn disrupt the CFD results in the near field. Monroy et al. (2010) and Marcer et al. (2007) used a coarse computational mesh to damp perturbation fields and prevent wave reflection. Here, we take a more general approach based on implicit relaxation zones described by Jasak et al. (2015). The relaxation zone volumetrically combines governing equations of the flow model and prescribed incident far field solution in order to force perturbation fields to vanish in the far field. This leaves clean incident flow near the boundaries and thus prevents wave reflection. The procedure shall be described on a general, SWENSE decomposed transport equation for a general variable $\xi = \xi_I + \xi_P$:

$$\frac{\partial (\rho \xi_P)}{\partial t} + \nabla \bullet (\rho \mathbf{u} \xi_P) - \nabla \bullet (\gamma_\xi \nabla \xi_P) + \frac{\partial (\rho \xi_I)}{\partial t} + \nabla \bullet (\rho \mathbf{u} \xi_I) - \nabla \bullet (\gamma_\xi \nabla \xi_I) - S_u = \mathcal{T}(\xi_P) = 0, \tag{26}$$

where γ_ξ is the diffusion coefficient and S_u a source term. $\mathcal{T}(\xi_P)$ denotes a general transport operator acting on the perturbation field ξ_P. The perturbation field should be zero at the boundaries, giving:

$$\xi_P = 0 \rightarrow \mathcal{R}(\xi_P) = 0, \tag{27}$$

where $\mathcal{R}(\xi_P)$ is the relaxation zone operator. Weight field w is used to blend two models represented by Eqs. (26) and (27). w is equal to 1 at the far field boundaries (Fig. 2), which forces the perturbation field to vanish. Toward the area of interest in the domain interior, w reduces smoothly to 0. A single equation can be written in terms of w and Eqs. (26) and (27):

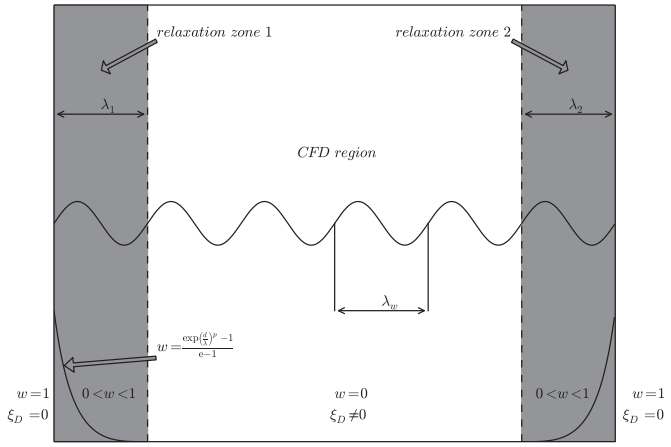

Fig. 2. Relaxation zones with weight field. White region represents full CFD domain, while shaded gray area represents relaxation zones. In relaxation zones, the solution is a linear combination of CFD and potential flow solution.

$$(1 - w)\mathcal{T}(\xi_P) + w\mathcal{R}(\xi_P) = 0. \tag{28}$$

This forces the perturbation field to vanish where $w=1$, and gives the full CFD solution for $w=0$. Following Jacobsen et al. (2012), w is chosen as:

$$w = \frac{e^{\left(\frac{d}{\lambda}\right)^p} - 1}{e - 1}, \tag{29}$$

where d is the shortest distance to the boundary and λ is the length of the relaxation zone. p is a spatial exponent, usually set to 3.5 (Jacobsen et al., 2012). The length of the relaxation zone should be sufficiently large to prevent any wave reflection. This is studied further in the accompanying paper.

In this study, velocity and LS fields are blended using implicit relaxation zones. Eq. (28) can be used to combine the governing equations in their decomposed form:

- Continuity equation, Eq. (17), becomes:

$$(1 - w)\left(\nabla \bullet \mathbf{u}_P + \nabla \bullet \mathbf{u}_I \right) = 0, \tag{30}$$

- Momentum equation, Eq. (18), becomes:

$$(1 - w)\left(\frac{\partial (\rho \mathbf{u}_P)}{\partial t} + \nabla \bullet (\rho \mathbf{u} \mathbf{u}_P) - \nabla \bullet (\mu_{eff} \nabla \mathbf{u}_P) \right) = (1 - w)\left(\frac{\partial (\rho \mathbf{u}_I)}{\partial t} - \nabla \bullet (\rho \mathbf{u} \mathbf{u}_I) + \nabla \bullet (\mu_{eff} \nabla \mathbf{u}_I) - \nabla p_d - \mathbf{g} \bullet \mathbf{x} \nabla \rho + \nabla \mathbf{u} \bullet \nabla \mu_{eff} + \sigma \kappa \nabla \alpha. \right) - w \mathbf{u}_P, \tag{31}$$

- LS transport equation, Eq. (25), becomes:

$$(1 - w)\left(\frac{\partial \psi_P}{\partial t} + \nabla \bullet (\mathbf{c} \psi_P) - \psi_P \nabla \bullet \mathbf{c} - b \nabla \bullet (\nabla \psi_P) \right) = (1 - w)\left(-\frac{\partial \psi_I}{\partial t} - \nabla \bullet (\mathbf{c} \psi_I) + \psi_I \nabla \bullet \mathbf{c} + b \nabla \bullet (\nabla \psi_I) + b \frac{\sqrt{2}}{\epsilon} \tanh\left(\frac{\psi}{\epsilon \sqrt{2}} \right) \right) - w \psi_P. \tag{32}$$

Additional sink terms in the momentum equation, Eq. (31), and the LS equation, Eq. (32), implicitly force $\mathbf{u}_P$ and ψ_P to vanish in the relaxation zone, where $w \neq 0$. This term is not present in the continuity equation, Eq. (30), because in the segregated solution algorithm $\mathbf{u}_P$ will already be equal to zero in the relaxation zone after the solution of the momentum equation.

5. Numerical model

The mathematical model is discretised in space using a second-order accurate, collocated FV method with support for arbitrary polyhedral (unstructured) grids (Jasak, 1996), Fig. 3. Unstructured, body-fitted grids are most often used for simulations of flows around ship hulls as they simplify mesh generation. The description of the numerical model is divided into the following parts: FV discretisation of governing equations, with the emphasis on derivation of the pressure equation; calculation of the diffusion coefficient in the LS equation; and the solution algorithm for the coupled equation set.

5.1. Finite Volume discretisation

The literature on basic FV discretisation is vast (Versteeg and Malalasekera, 1995; Ferziger and Peric, 1996; Jasak, 1996; Rusche, 2002), and will not be described here in detail. Following notation by Rusche (2002), terms enclosed within square brackets $[\cdot]$ are treated implicitly, while other terms are discretised explicitly. Explicit terms include:

1. contributions arising from the incident field, known at every time-step;
2. other contributions for which the values at the previous time-step or iteration are used.

5.1.1. Momentum equation

The discretised momentum equation, Eq. (31), has the following form:

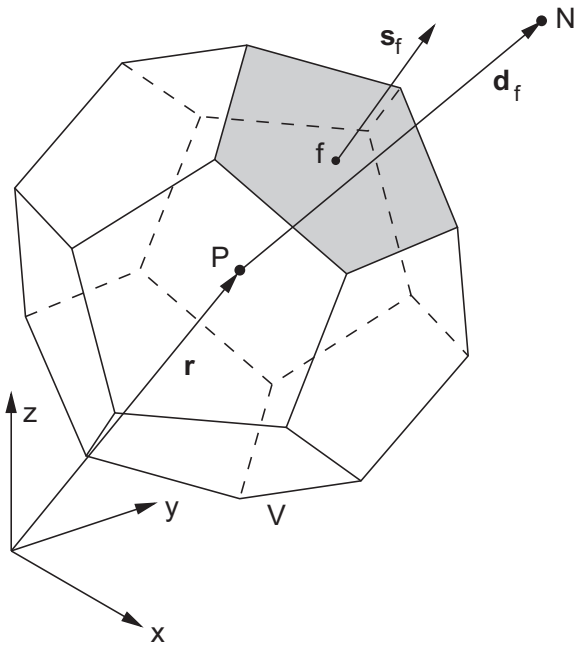

Fig. 3. Polyhedral control volume. Control volume *P* shares a common face with its neighbour *N*.

$$
\begin{aligned}
&(1-w)\left(\left[\frac{\partial(\rho\mathbf{u}_P)}{\partial t}\right] + [\nabla\bullet(\rho\mathbf{u}\mathbf{u}_P)] - [\nabla\bullet(\mu_{eff}\nabla\mathbf{u}_P)]\right)\\
&\quad = (1-w)\left(\frac{\partial(\rho\mathbf{u}_I)}{\partial t} - \nabla\bullet(\rho\mathbf{u}\mathbf{u}_I) + \nabla\bullet(\mu_{eff}\nabla\mathbf{u}_I) - \nabla p_d - \mathbf{g}\bullet\mathbf{x}\nabla\rho\right.\\
&\qquad \left. + \nabla\mathbf{u}\bullet\nabla\mu_{eff} + \sigma\kappa\nabla\alpha\right) - w[\mathbf{u}_P],
\end{aligned}
\tag{33}
$$

Time derivative, convection, diffusion and sink term for the perturbation field are discretised implicitly. Using Eq. (33), a linear equation for each control volume is assembled:

$$a_P\mathbf{u}_{P,P} + \sum_f a_N\mathbf{u}_{P,N} = \mathbf{S}, \tag{34}$$

where a_P represents the diagonal coefficient and a_N represent off-diagonal coefficients for a control volume "*P*". $\sum_f$ denotes sum over all neighbouring faces. Index "*P*, *P*" marks the perturbation velocity field at the control volume "*P*", and similarly *P*, *N* marks the perturbation velocity field at the control volume "*N*". **S** is the source term arising from explicit terms on the RHS of Eq. (33) and possible non-orthogonal correction in the diffusion term. Boundary cells have additional diagonal or source contributions depending on boundary conditions (Jasak, 1996).

In this work, the following discretisation schemes for terms in the momentum equation, Eq. (30), are used:

- Linear blend of Crank–Nicholson (Ubbink, 1997) and implicit Euler (Versteeg and Malalasekera, 1995) for time derivative terms.
- Compact stencil second-order linear-upwind scheme for convection terms.
- Linear interpolation with an explicit non-orthogonal correction (Jasak, 1996) for diffusion terms.
- Basic linear interpolation for other terms.

Second-order accurate schemes in space are used for the momentum equation. A blend of first-order Euler and second order Crank–Nicholson scheme for time derivatives proved to be both stable and sufficiently accurate.

5.1.2. Pressure equation

In segregated solution algorithms for incompressible flows, the pressure equation is used to create conservative fluxes, obeying the continuity equation, Eq. (17). Following Patankar and Spalding (1972) and Jasak (1996), the derivation of the pressure equation starts from the semi-discretised form of the momentum equation, Eq. (34):

$$a_P\mathbf{u}_{P,P} = \mathbf{H}(\mathbf{u}_P) - \nabla p_d, \tag{35}$$

where the pressure gradient term is left undiscretised in analogous to Rhie and Chow (1983) correction. This equation is obtained from the integral form of the blended, SWENSE decomposed momentum equation, Eq. (33), using the discretisation schemes described above. The equation is divided by the cell volume to enable face interpolation of the matrix coefficients. The $\mathbf{H}(\mathbf{u}_P)$ term consists of two parts:

1. the transport part, which includes the matrix coefficients for all neighbours multiplied by the corresponding velocities;
2. the source part which includes all the source terms arising from SWENSE decomposition (incident wave field), gradient of the density, gradient of the effective viscosity, surface tension force and terms related to the discretisation of the time derivative term of the perturbation velocity field.

The discretised form of the continuity equation, Eq. (30), reads:

$$(1-w)\left(\sum_f \mathbf{s}_f \cdot \mathbf{u}_{P,f} + \sum_f \mathbf{s}_f \cdot \mathbf{u}_{I,f}\right) = 0. \tag{36}$$

Index "f" denotes a value at the face centre, while indices "P" and "I" stand for perturbation and incident field respectively. The semi-discretised momentum equation, Eq. (35), is used to express the perturbation velocity field:

$$\mathbf{u}_{P,P} = \frac{\mathbf{H}(\mathbf{u}_P)}{a_P} - \frac{1}{a_P}\nabla p_d. \tag{37}$$

The perturbation velocity at the face centre is obtained by linear interpolation of the cell-centre velocities, Eq. (37):

$$\mathbf{u}_{P,f} = \left(\frac{\mathbf{H}(\mathbf{u}_P)}{a_P}\right)_f - \left(\frac{1}{a_P}\right)_f (\nabla p_d)_f, \tag{38}$$

where Eq. (38) is later used to calculate face fluxes given a new pressure field p_d that enforces the continuity equation.

Substituting perturbation velocities interpolated to cell faces given by Eq. (38) into the discretised form of the continuity equation, Eq. (36), yields the pressure equation:

$$\begin{aligned}\nabla\cdot\left(\frac{1}{a_P}\nabla p_d\right) &= (1-w)\left(\nabla\cdot\left(\frac{\mathbf{H}(\mathbf{u}_P)}{a_P}\right) + \nabla\cdot\mathbf{u}_I\right)\\ &= (1-w)\left(\sum_f \mathbf{s}_f\cdot\left(\frac{\mathbf{H}(\mathbf{u}_P)}{a_P}\right)_f + \sum_f \mathbf{s}_f\cdot\mathbf{u}_{I,f}\right),\end{aligned} \tag{39}$$

The $(1-w)$ blending pre-factor multiplying the pressure Laplacian term is omitted because pressure p_d is not decomposed using the SWENSE method. In contrast to a non-decomposed incompressible pressure equation, Eq. (39) has one additional source term coming from the divergence of the incident wave field. As discussed in the previous section, this term vanishes on a differential or numerical level (depending on the method used to obtain the incident wave field). For example, if the incident wave field is calculated from first order Stokes' theory, the Laplacian equation for the velocity potential causes $\nabla\cdot\mathbf{u}_I$ to vanish. Mapping this analytical solution to a FV mesh would cause continuity errors because $\nabla\cdot\mathbf{u}_I = \sum_f \mathbf{s}_f\cdot\mathbf{u}_{I,f} \neq 0$. This also applies for more advanced numerical models for the incident wave field since the solution of the governing equations is obtained on an arbitrary computational grid. This is illustrated in Fig. 4. The figure depicts an initial wave field obtained by stream function wave theory (Rienecker and Fenton, 1981). This field mapped on a FV mesh provides α and $\mathbf{u}_I$ distribution. The continuity error $\nabla\cdot\mathbf{u}_I = \sum_f \mathbf{s}_f\cdot\mathbf{u}_{I,f}$ is calculated for each cell. The FV method presented in this work is strongly conservative, hence $\nabla\cdot\mathbf{u}_I$ should ideally be as small to machine tolerance. As shown in Fig. 4, this is not achieved; this could be remedied by a choice of interpolation scheme for $\mathbf{u}_{I,f}$ which satisfies the continuity equation for the incident velocity field. In this study, this term is included in the pressure equation. Thus, the non-decomposed pressure field, and consequently the perturbation velocity field, will make up for the non-conservative nature of the incident velocity field.

The $(1-w)$ blending pre-factor accounts for continuity errors in the relaxation zone. Without this term, the continuity would be enforced inside the relaxation zone through p_d and consequently through $\mathbf{u}_D$, see Eq. (38), in contradiction with the momentum equation, Eq. (33), where $\mathbf{u}_D$ is forced to gradually vanish in the relaxation zone near the boundary. Hence, this term causes the pressure to be zero inside relaxation zones. This is considered acceptable since the pressure inside relaxation zones can be easily reconstructed using the pressure from the incident wave field. However, such procedure should be unnecessary because the area of interest is not located within the relaxation zone.

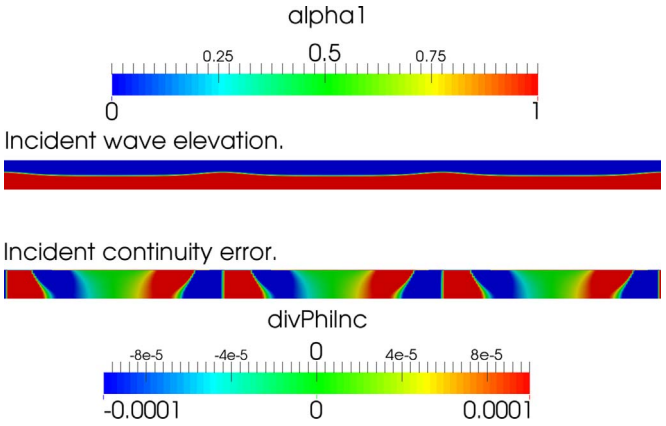

Fig. 4. Initial field obtained by stream function wave theory (Rienecker and Fenton, 1981) mapped on a FV mesh. The above figure denotes the α distribution and the figure below denotes the continuity error, $\nabla\cdot\mathbf{u}_I = \sum_f \mathbf{s}_f\cdot\mathbf{u}_{If}$.

The final form of the discretised pressure–velocity system reads:

- Discretised momentum equation:

$$a_P\mathbf{u}_{P,P} = \mathbf{H}(\mathbf{u}_P) - \sum_f \mathbf{s}_f p_{df}, \tag{40}$$

- Discretised pressure equation:

$$\begin{aligned}&\sum_f \mathbf{s}_f\cdot\left(\frac{1}{a_P}\right)_f (\nabla p_d)_f\\ &= (1-w)\left(\sum_f \mathbf{s}_f\cdot\left(\frac{\mathbf{H}(\mathbf{u}_P)}{a_P}\right)_f + \sum_f \mathbf{s}_f\cdot\mathbf{u}_{I,f}\right).\end{aligned} \tag{41}$$

Although a coupled approach for the solution of the pressure–velocity system is possible in the FV method (Darwish et al., 2009; Darwish and Moukalled, 2014), a segregated algorithm is used in this study. The algorithm is based on a combination of SIMPLE (Patankar and Spalding, 1972) and PISO (Issa, 1986) algorithms as detailed below.

After solving the pressure equation, Eq. (41), the total face flux is calculated as:

$$F = \mathbf{s}_f\cdot(\mathbf{u}_{P,f} + \mathbf{u}_{I,f}) = \mathbf{s}_f\cdot\left(\left(\frac{\mathbf{H}(\mathbf{u}_P)}{a_P}\right)_f - \left(\frac{1}{a_P}\right)_f (\nabla p_d)_f + \mathbf{u}_{I,f}\right). \tag{42}$$

When the pressure equation, Eq. (41), is satisfied, volumetric face fluxes are conservative in the discrete form: $\sum_f F = 0$. Fluxes are used to convect the LS field and all other transported variables, e.g. in the turbulence model.

5.1.3. Level set equation

The blended, SWENSE-decomposed LS transport equation, Eq. (32), is discretised as:

$$\begin{aligned}&(1-w)\left(\left[\frac{\partial\psi_P}{\partial t}\right] + [\nabla\cdot(\mathbf{c}\psi_P)] - [\psi_P\nabla\cdot\mathbf{c}] - [b\nabla\cdot(\nabla\psi_P)]\right)\\ &= (1-w)\left(-\frac{\partial\psi_I}{\partial t} - \nabla\cdot(\mathbf{c}\psi_I) + \psi_I\nabla\cdot\mathbf{c} + b\nabla\cdot(\nabla\psi_I)\right.\\ &\quad \left. + b\frac{\sqrt{2}}{\epsilon}\tanh\left(\frac{\psi}{\epsilon\sqrt{2}}\right)\right) - w[\psi_P],\end{aligned} \tag{43}$$

where $\mathbf{c}$ is defined with Eqs. (20) and (22):

$$\mathbf{c} = \mathbf{u} + \mathbf{w}_1 + \mathbf{w}_2 = \mathbf{u} + b\frac{\sqrt{2}}{\epsilon}\tanh\left(\frac{\psi}{\epsilon\sqrt{2}}\right)\nabla\psi + b\kappa\frac{\nabla\psi}{|\nabla\psi|}. \tag{44}$$

Terms on the LHS of Eq. (43) are discretised implicitly. The sink term for the implicit blending procedure on the RHS of equation is also treated implicitly, increasing the diagonal dominance of the matrix. This term forces the perturbation LS field to vanish in the relaxation zone near the far field boundaries. Other terms are explicit, as the incident LS field is known at each time-step.

The following discretisation schemes used in Eq. (43) are:

- Linear blend of Crank–Nicholson (Ubbink, 1997) and implicit Euler (Versteeg and Malalasekera, 1995) for time derivative terms.
- Second-order accurate Total Variation Diminishing scheme (TVD) (Hirsch, 1984) with van Leer's (1977) flux limiter in deferred correction form (Ferziger and Peric, 1996).
- Linear interpolation with an explicit non-orthogonal correction (Jasak, 1996) for diffusion terms.

5.2. Determination of the diffusion coefficient in the Level Set equation

The parameter b appearing in the LS transport equation, Eq. (43), acts as a diffusion coefficient and a pre-factor for curvature driven terms, see Section 2. In the absence of curvature driven motion, the choice of b is purely numerical (Sun and Beckermann, 2007). Sun and Beckermann (2007) used a Courant–Friedrichs–Lewy (CFL) condition for the PF equation to determine this parameter. We apply a similar approach, with the following assumptions:

- b should be as small as possible in order to keep a sharp interface, preventing excessive diffusion;
- maximum CFL number is not limited to 1 because Eq. (43) is treated implicitly;
- b should be calculated using arbitrary polyhedral FV method and its conventions.

We define the convective CFL number in the LS transport equation as:

$$CFL_c = \frac{\mathbf{s}_f \cdot \mathbf{c}_f}{\mathbf{s}_f \cdot \mathbf{d}_f}\Delta t, \tag{45}$$

where $\mathbf{c}_f$ is the face interpolated value of the convective velocity field in the LS transport equation as indicated in Eq. (24). Consequently, the CFL number due to diffusive flux can be defined as:

$$CFL_d = b\frac{\mathbf{s}_f \cdot \nabla\psi_f}{\mathbf{s}_f \cdot \mathbf{d}_f}\Delta t, \tag{46}$$

where $\nabla\psi_f$ is the surface normal LS gradient. The sum of both CFL numbers should not exceed the specified CFL_ψ limit:

$$CFL_c + CFL_d \leq CFL_\psi, \tag{47}$$

where $CFL_\psi = 1$ in case of explicit solution schemes. This inequality gives an upper bound for b.

During the solution process, the time-step is controlled with a designated CFL number based on the fluid flow:

$$CFL = \frac{\mathbf{s}_f \cdot \mathbf{u}_f}{\mathbf{s}_f \cdot \mathbf{d}_f}\Delta t, \tag{48}$$

where $\mathbf{s}_f \cdot \mathbf{u}_f$ is the volumetric face flux. Numerical tests have shown that $CFL_\psi \approx 2$ CFL yields good results, even though a solution can be achieved with higher values. This is demonstrated in the accompanying paper. Nevertheless, b is numerically a diffusion coefficient. Even though it is purely a numerical parameter, $b \geq 0$ is required for numerical stability.

The parameter b should be as small as possible in the absence of curvature-driven motion to prevent excessive smearing of the interface. For this reason, b is divided by a stabilisation constant $\gamma \geq O(10^5)$. Finally, an expression for b can be derived as:

$$b = \frac{b^o}{\gamma}\frac{CFL_\psi - CFL_c}{CFL_d}, \tag{49}$$

where b^o denotes the parameter b from the previous iteration or time-step. The constant γ is a purely numerical parameter whose exact value has minor influence on the solution as the study presented in the accompanying paper demonstrates.

5.3. Solution algorithm

The segregated solution algorithm used in this work is a combination of SIMPLE (Patankar and Spalding, 1972) and PISO (Issa, 1986) algorithms. A flow chart of the solution procedure for each time step is given in Fig. 5. At the beginning of every time step, incident wave fields, $\mathbf{u}_I$ and ψ_I, are calculated from potential wave theory. Coupling between ψ_P, $\mathbf{u}_P$ and p_d is achieved in a segregated manner using a SIMPLE loop. The SIMPLE loop begins with an update of parameter b for the LS equation, Eq. (43). Parameter b is updated based on the latest CFL_c and CFL_d numbers. The perturbation equation for ψ_P is assembled and solved. ψ is then updated as $\psi = \psi_P + \psi_I$. To update the density with Eq. (1), α is obtained from the hyperbolic tangent reconstruction, Eq. (14). The subsequent PISO loop handles the pressure–velocity coupling. The momentum equation, Eq. (40), is solved using the pressure gradient from the previous iteration. The divergence-free velocity field is then obtained by solving the pressure equation, Eq. (41), and updating the perturbation velocity field and face flux field, Eqs. (37) and (42), respectively. Convergence of the PISO loop is not tested: the user specifies a fixed number of PISO correctors. If enabled, equations for turbulence models are solved and the effective dynamic viscosity μ_{eff} is updated. The SIMPLE loop ends if the number of specified SIMPLE correctors is exceeded. This is repeated until the simulation reaches the end time.

In this work, four SIMPLE correctors and one PISO corrector are used. The linear system resulting from pressure equation, Eq. (41), is solved using the algebraic multi-grid (AMG) (Weiss et al., 1999) solver with the ILU smoother. Other equations are hyperbolic, and are solved with a stabilised Bi-conjugate gradient Krylov subspace solver (BiCGStab) (Saad, 2003). Under-relaxation factors are not used.

6. Summary

A solution and domain decomposition model for two-phase flows is described. The model is primarily intended for simulations containing wave-like phenomena in naval hydrodynamics applications.

Interface capturing is achieved with the LS method derived from the PF equation; there is no need to additionally redistance the LS field after transport.

The solution is decomposed using the SWENSE method, where the field is divided into incident and perturbation components. The incident wave field is obtained with low-cost potential flow wave theories, while the perturbation component is solved for. The perturbation component accounts for two-phase, non-linear, viscous, diffraction and possibly radiation effects not accounted for in the incident flow field. Only the velocity and the LS fields are

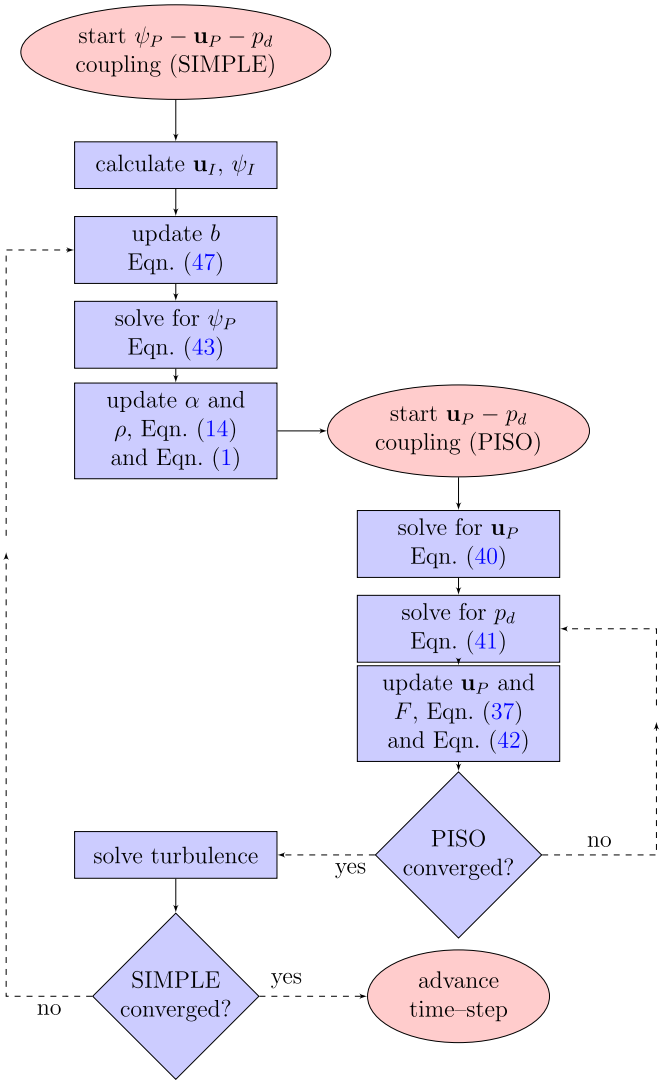

Fig. 5. Flow chart of the segregated solution algorithm.

decomposed in the presented approach. The pressure is not decomposed for efficiency reasons.

The domain is decomposed using the relaxation zones. Relaxation zones damp the perturbation field near the boundaries, which leaves only the potential flow solution. This is necessary to prevent unwanted wave reflection, which would disrupt CFD results. Damping of the perturbation fields is achieved implicitly within the governing equations.

In this paper, the one-way coupling between the incident flow and CFD solution is implied. However, it is important to note that the present model enables easy extension towards the two-way coupling between a full CFD solution and the arbitrary incident flow model. An extension towards more advanced potential flow incident models (as used by Fredriksen et al., 2014; Zhang et al., 2014), incident potential flow depending on the CFD solution in the near field, is the topic of future work.

The solution algorithm is based on a second-order accurate, polyhedral FV method. All governing equations are discretised implicitly, which ensures numerical stability for $CFL \geq 1$. A single pressure equation is derived, which makes the total flux conservative by updating only the perturbation velocity field. The solution procedure is a combination of segregated SIMPLE and PISO algorithms that use a fixed number of PISO correctors and SIMPLE correctors.

A detailed verification and validation of the model are presented in accompanying paper.

Acknowledgements

This research was sponsored by Bureau Veritas and Hyundai Heavy Industries under the administration of Dr. Šime Malenica and Dr. Geon-Hong Kim. The third author acknowledges the support of the National Research Foundation of Korea (NRF) grant funded by the Korea Government (MSIP) through GCRC-SOP (Grant No. 2011-0030013).

Appendix A. Picard linearisation of the hyperbolic tangent source term

Below, we show the Picard linearisation procedure of the hyperbolic tangent source term in the LS transport equation, Eq. (25). The source term can be written in the following form:

$$S(\psi) = b\frac{\sqrt{2}}{\epsilon}\tanh\left(\frac{\psi}{\epsilon\sqrt{2}}\right) = a_1\tanh(a_2\psi), \tag{A.1}$$

where a_1 and a_2 are non-negative constants, since $b \geq 0$ and $\epsilon \geq 0$. Expanding the above expression in the Taylor series around the value from the previous time-step ψ^o gives:

$$S(\psi^n) = S(\psi^o) + \left(\frac{\partial S}{\partial \psi}\right)^o(\psi^n - \psi^o), \tag{A.2}$$

with

$$\left(\frac{\partial S}{\partial \psi}\right)^o = a_1 a_2\,\mathrm{sech}^2(a_2\psi^o). \tag{A.3}$$

Substituting Eq. (A.3) into Eq. (A.2) yields a linearised version of the source term:

$$\begin{aligned} S(\psi^n) &= a_1\tanh(a_2\psi^o) + a_1 a_2\,\mathrm{sech}^2(a_2\psi^o)\left(\psi^n - \psi^o\right) \\ &= S_1 + S_u\psi^n - S_u\psi^o. \end{aligned} \tag{A.4}$$

This procedure divides the source term into three parts. Terms S_1 and $S_u\psi^o$ are explicit since they are bound to the value of ψ_o from the previous time-step. The second term can be made implicit. However, S_u appearing on the RHS of the LS transport equation, Eq. (25), is non-negative. For implicit treatment, this term would have to be transferred to the LHS of the equation, making S_u negative. Hence, an additional diagonal contribution of $-S_u$ would decrease the diagonal dominance of the resulting matrix, so this is omitted.

References

Brackbill, J.U., Kothe, D.B., Zemach, C., 1992. A continuum method for modelling surface tension. J. Comput. Phys. 100, 335–354.
Darwish, M., Moukalled, F., 2014. A fully coupled Navier-Stokes solver for fluid flow at all speeds. Numer. Heat Transf. Part B 65, 410–444.
Darwish, M., Sraj, I., Moukalled, F., 2009. A coupled finite volume solver for the solution of incompressible flows on unstructured grids. J. Comput. Phys. 228, 180–201.
Dommermuth, D.G., Yue, D.K.P., 1987. A high-order spectral method for the study of nonlinear gravity waves. J. Fluid Mech. 184, 267–288.
Ducrozet, Guillaume, Engsig-Karup, Allan P., Bingham, Harry B., Ferrant, Pierre, 2014. A non-linear wave decomposition model for efficient wave–structure interaction. Part A: Formulation, validations and analysis. J. Comput. Phys. 257, 863–883.
Feng, X., Bai, W., 2015. Wave resonances in a narrow gap between two barges using fully nonlinear numerical simulation. Appl. Ocean Res. 50, 119–129.
Ferrant, P., Gentaz, L., Le Touzé, D., 2002. A new RANSE/potential approach for water wave diffraction. In: Proceedings of Numerical Towing Tank Symposium, NuTTS, September.

Ferziger, J.H., Peric, M., 1996. Computational Methods for Fluid Dynamics. Springer, Berlin.
Folch, R., Casademunt, J., Hernández-Machado, A., 1999. Phase-field model for Hele–Shaw flows with arbitrary viscosity contrast. I. Theoretical approach. Phys. Rev. E 60, 1724.
Fredriksen, Arnt G., Kristiansen, Trygve, Faltinsen, Odd M., 2014. Experimental and numerical investigation of wave resonance in moonpools at low forward speed. Appl. Ocean Res. 47, 28–46.
Gómez, P., Hernández, J., López, J., 2005. On the reinitialization procedure in a narrow-band locally refined level set method for interfacial flows. Int. J. Numer. Methods Eng. 63, 1478–1512.
Hartmann, D., Meinke, M., Schröder, W., 2008. Differential equation based constrained reinitialization for level set methods. J. Comput. Phys. 227, 6821–6845.
Higuera, P., Lara, J.L., Losada, I.J., 2013a. Realistic wave generation and active wave absorption for Navier–Stokes modelsapplication to OpenFoam®. Coast. Eng. 71, 102–118. http://dx.doi.org/10.1016/j.coastaleng.2012.07.002.
Higuera, P., Lara, J.L., Losada, I.J., 2013b. Simulating coastal engineering processes with OpenFoam®. Coast. Eng. 71, 119–134. http://dx.doi.org/10.1016/j.coastaleng.2012.06.002.
Hirsch, C., 1984. Numerical Computation of Internal and External Flows. Computational Methods for Inviscid and Viscous Flows, vol. 2. John Wiley & Sons, Chichester.
Huang, J., Carrica, P.M., Stern, F., 2007. Coupled ghost fluid/two-phase level set method for curvilinear body-fitted grids. Int. J. Numer. Methods Fluids 44, 867–897. http://dx.doi.org/10.1002/fld.1499.
Issa, R.I., 1986. Solution of the implicitly discretised fluid flow equations by operator-splitting. J. Comput. Phys. 62, 40–65.
Jacobsen, N.G., Fuhrman, D.R., Fredsøe, J., 2012. A wave generation toolbox for the open-source CFD library: OpenFoam®. Int. J. Numer. Methods Fluids 70 (9), 1073–1088. http://dx.doi.org/10.1002/fld.2726.
Jasak, H., 1996. Error Analysis and Estimation for the Finite Volume Method with Applications to Fluid Flows (Ph.D. thesis). Imperial College of Science, Technology & Medicine, London.
Jasak, H., Vukčević, V., Gatin, I., 2015. Numerical Simulation of Wave Loads on Static Offshore Structures. in: CFD for Wind and Tidal Offshore Turbines, Springer Tracts in Mechanical Engineering, Cham, pp. 95–105. ISBN 978-3-319-16201-0, http://dx.doi.org/10.1007/978-3-319-16202-7.
Kleefsman, T., 2005. Water Impact Loading on Offshore Structures (Ph.D. thesis). Rijks universiteit Groningen.
Larsson, L., Stern, F., Vissoneau, M., 2013. Numerical Ship Hydrodynamics: An assessment of the Gothenburg 2010 Workshop. Springer, Dordrecht. http://dx.doi.org/10.1007/978-94-007-7189-5.
Luppes, R., Düz, B., van der Heiden, H.J.L., van der Plas, P., Veldman, A.E.P., September 2012. Numerical simulations of two-phase flow with COMFLOW: past and recent developments. in: Proceedings of the ECCOMAS. pp. 1–16.
Marcer, R., Audiffren, C., Dassibat, C., de Jouette, C., Guillerm, P.E., April 2007. Seakeeping modelling in calm water and in waves using the CFD code Eole. in: 11ème Journées de l'Hydrodynamique, pp. 1–12.
Monroy, C., Ducrozet, G., Bonnefoy, A., Babarit, A., Ferrant, P., 2010. RANS simulations of a CALM buoy in regular and irregular seas using the SWENSE method. in: Proceedings of the Twentieth International Off-shore and Polar Engineering Conference, pp. 678–685, June.
Osher, S., Fedkiw, R., 2003. Level Set Methods and Dynamic Implicit Surfaces. Springer, New York.
Patankar, S.V., 1980. Numerical Heat Transfer and Fluid Flow. Taylor and Francis, Washington.
Patankar, S.V., Spalding, D.B., 1972. A calculation procedure for heat, mass and momentum transfer in three-dimensional parabolic flows. Int. J. Heat Mass Transf. 15, 1787–1806.
Rhie, C.M., Chow, W.L., 1983. A numerical study of the turbulent flow past an isolated airfoil with trailing edge separation. AIAA J. 21, 1525–1532.
Rienecker, M.M., Fenton, J.D., 1981. A Fourier approximation method for steady water waves. J. Fluid Mech. 104, 119–137.
Rusche, H., 2002. Computational Fluid Dynamics of Dispersed Two - Phase Flows at High Phase Fractions (Ph.D. thesis). Imperial College of Science, Technology & Medicine, London.
Saad, Y., 2003. Iterative Methods for Sparse Linear Systems, 2nd edition. Society for Industrial and Applied Mathematics Philadelphia, SIAM, Philadelphia.
Sethian, J.A., 1996. Level Set Methods: Evolving Interfaces in Geometry, Fluid Mechanics, Computer Vision and Materials Science. Cambridge University Press, Cambridge.
Stern, F., Yang, J., Wang, Z., Sadat-Hosseini, H., Mousaviraad, M., Bhushan, S., Xing, T., 2012. Computational ship hydrodynamics: nowadays and way forward. in: Proceedings of the 29th Symposium on Naval Hydrodynamics, pp. 1–73, August.
Sun, Y., Beckermann, C., 2007. Sharp interface tracking using the phase-field equation. J. Comput. Phys. 220, 626–653. http://dx.doi.org/10.1016/j.jcp.2007.05.025.
Sun, Y., Beckermann, C., 2008. A two-phase diffusive-interface model for Hele–Shaw flows with large property contrasts. Physica D 237, 3089–3098. http://dx.doi.org/10.1016/j.physd.2008.06.010.
Sussman, M., Fatemi, E., 1999. An efficient, interface-preserving level set redistancing algorithm and its application to interfacial incompressible fluid flow. SIAM J. Sci. Comput. 20 (4), 1165–1191.
Tryggvason, G., Scardovelli, R., Zaleski, S., 2011. Direct Numerical Simulations of Gas–Liquid Multiphase Flows. Cambridge University Press, Cambridge.
Ubbink, O., 1997. Numerical Prediction of Two Fluid Systems with Sharp interfaces (Ph.D. thesis). Imperial College of Science, Technology & Medicine, London.
Ubbink, O., Issa, R.I., 1999. A method for capturing sharp fluid interfaces on arbitrary meshes. J. Comput. Phys. 153, 26–50.
van Leer, B., 1977. Towards the ultimate conservative difference scheme. IV. A new approach to numerical convection. J. Comput. Phys. 23, 276–299.
Versteeg, H.K., Malalasekera, W., 1995. An introduction to Computational Fluid Dynamics: The Finite Volume Method. Pearson Education Limited, Glasgow.
Vukčević, V., Östman, A., Jasak, H., December 2014. Rapid Simulations of pure sway motion using FVM in OpenFOAM. In: SIMMAN 2014: Workshop on Verification and Validation of Ship Manoeuvring Simulation Methods.
Weiss, J.M., Maruszewski, J.P., Smith, W.A., 1999. Implicit solution of preconditioned Navier–Stokes equations using algebraic multigrid. AIAA J. 37 (1), 29–36.
Weller, H.G., Tabor, G., Jasak, H., Fureby, C., 1998. A tensorial approach to computational continuum mechanics using object oriented techniques. Comput. Phys. 12, 620–631.
West, B.J., Brueckner, K.A., Janda, R.S., 1987. A new numerical method for surface hydrodynamics. J. Geophys. Res. 92 (C11), 11803–11824.
Wilcox, D.C., 1993. Turbulence Modeling for CFD. DCW Industries.
Zhang, Yi., Del Pin, Facundo, Yim, Solomon C., 2014. A heterogeneous flow model based on DD method for free surface fluid–structure interaction problems. Int. J. Numer. Methods Fluids 74 (4), 292–312.